BBAA VI International Colloquium on:
Bluff Bodies Aerodynamics & Applications
Milano, Italy, July, 20-24 2008

DIAGNOSIS OF FATIGUE COLLAPSES OF SLENDER STRUCTURES DUE TO AERODYNAMIC WIND ACTIONS

Maria Pia Repetto[*] and Giovanni Solari[*]

[*]DICAT, Department of Civil, Environmental and Architectural Engineering
University of Genoa, Via Montallegro 1, Genova Italy
e-mail: repetto@dicat.unige.it

Keywords: Alongwind response, Crosswind response, Fatigue, Vortex shedding.

Abstract. *The authors of this paper have recently proposed a complete procedure for the wind-induced fatigue analysis of slender structures for general wind conditions. This paper adopts the proposed procedure to analyze the wind-induced collapses of two slender structures. The application of the proposed method, compared with the examined real cases, leads to accurate fatigue life prediction; moreover, it gives a complete picture of the stress state and damage of the structures, furnishing useful information on the structural behavior and a key for the interpretation of collapses and damage causes. In particular, the analysis highlights the critical aspects of the aerodynamic behavior of the considered structures and suggests some remarks on the current state-of-the art of design against wind-induced actions.*

1 INTRODUCTION

Wind-structure interaction implies complex aerodynamic phenomena which result in alongwind, crosswind and torsional actions. Since these actions may produce large vibrations at moderate and frequent wind velocities, structures may undergo a great number of stress cycles leading to damage accumulation. Several damage and even collapses have been observed for different kinds of structures such as urban light poles [1, 2, 3], guyed masts and chimneys [4, 5]. Notwithstanding this, literature is still fragmented and there is a lack of reliable engineering and standards methods for wind-induced fatigue analysis.

Since 2000, the authors of this paper have developed a wide research project aimed at formulating and calibrating a general procedure for determining the mean fatigue damage and the mean fatigue life of structures under general wind loading conditions [6-11]. The proposed method takes into account the joint probability distribution of the mean wind velocity, of wind direction and of thermal atmospheric stratification at the structural site; the wind-induced stress processes are determined considering the simultaneous alongwind, crosswind and torsional actions, and the possible occurrence of lock-in effects. The results include the stress cycles histogram, the mean total damage and the mean fatigue life obtained according to three cycle counting methods corresponding, respectively, to an upper, a lower bound and a good approximation of the fatigue damage.

The proposed method has been adopted to analyze the wind-induced collapses of two real slender structures, a ten meters anemometric pole and a thirty meters antennas tower. The structures are characterized by very simple structural scheme and satisfy the national and international Structural Codes from the ultimate limit state point of view. However, they both exhibited premature collapses due to wind-induced fatigue damage. The application of the proposed method gives a complete and clear picture of the stress state and damage of the structures, furnishing useful information on the structural behavior and a key for the interpretation of collapse and damage causes. The comparison between the predicted and the exhibited fatigue life confirms the reliability of the proposed method; moreover, the discussion of the results furnishes relevant remarks on the limits of the actual standards in wind-induced analysis from the fatigue point of view.

2 WIND-INDUCED EFFECTS AND FATIGUE ANALYSIS

Let us consider a structure or a structural element whose length ℓ is much greater than the reference size b of its cross-section. The incoming wind field is dealt with as a 3-variate random vector whose components are the mean wind velocity $\overline{u}_r$, evaluated at height r above the ground, the wind direction φ and the inverse of the Monin-Obukhov length (1/L) [11]. Time t is subdivided into successive ΔT intervals falling within the spectral gap, in which the three components are constant. When a time interval T greater than ΔT is taken into account, the wind loading effects induced in the structure are treated as a series of loading conditions, each corresponding to a ΔT step.

Let us introduce a series of velocity intervals $\Delta\overline{u}_i$ (i=1,2…), a series of directional sectors $\Delta\varphi_j$ (j=1,2, …, N) and a series of inverse Monin-Obukhov intervals $\Delta(1/L)_h$ (h=0,±1, ±2…). A structure is said to undergo the ijh-th loading condition when $\overline{u}_r \in \Delta\overline{u}_i$, $\varphi \in \Delta\varphi_j$ and $(1/L) \in \Delta(1/L)_h$. Thus, the ijh-th loading condition is characterized by the probability $P_{ijh}=P[\overline{u}_r \in \Delta\overline{u}_i \cap \varphi \in \Delta\varphi_j \cap 1/L \in \Delta(1/L)_h]$. This quantity is linked with the territorial position, with the local site properties and with the thermal atmospheric stratification [11].

The aerodynamic wind action in the ijh-th loading condition is modelled as a stochastic stationary Gaussian process and it is defined by the relationship:

$$F_{\alpha ijh}(z,t) = \overline{F}_{\alpha ijh}(z) + F'_{\alpha ijh}(z,t) \qquad (\alpha=x,y,\theta) \tag{7}$$

where z belongs to the range 0 to ℓ, F_{xijh} and F_{yijh} are the alongwind and crosswind forces, $F_{\theta ijh}$ is the torsional moment; $\overline{F}_{\alpha ijh}$ is the mean value of $F_{\alpha ijh}$, $F'_{\alpha ijh}$ is the nil mean fluctuation of $F_{\alpha ijh}$ around $\overline{F}_{\alpha ijh}$. Dealing with the structure as a linear system, the wind-induced stress in a point M of the structural cross-section at the coordinate z in the ijh-th loading condition is a stochastic stationary Gaussian process defined as:

$$s_{ijh}(M,t) = \overline{s}_{ijh}(M) + s'_{ijh}(M,t) \tag{8}$$

where $\overline{s}_{ijh}$ is the mean stress caused by $\overline{F}_{\alpha ijh}$, s'_{ijh} is the nil mean fluctuating stress caused by $F'_{\alpha ijh}$; this latter quantity is schematised as a bi-modal process [9-10] and expressed as:

$$s'_{ijh}(M,t) = s'_{Qijh}(M,t) + s'_{Dijh}(M,t) \tag{9}$$

where s'_{Qijh} is the low frequency quasi-static part of s'_{ijh}; s'_{Dijh} is the resonant part of s'_{ijh}, considered here as associated with only one mode of vibration whose natural frequency n^s_{Dijh} is much greater than the expected frequency ν^s_{Qijh} of s'_{Qijh}. Thus, the quasi-static and the resonant parts of the stress may be considered as uncorrelated, and the power spectral density function of s'_{ijh} is given by:

$$S^s_{ijh}(M,n) = S^s_{Qijh}(M,n) + S^s_{Dijh}(M,n) \tag{10}$$

where n is the frequency, S^s_{Qijh} and S^s_{Dijh} being the power spectral density functions of the quasi-static and of the resonant parts of the stress, respectively.

Based on this hypothesis, the variance and the expected frequency of the wind-induced stress in the ijh-th loading condition can be expressed as:

$$\left(\sigma^s_{ijh}\right)^2 = \left(\sigma^s_{Qijh}\right)^2 + \left(\sigma^s_{Dijh}\right)^2;\ \nu^s_{ijh} = \sqrt{\left(\nu^s_{Qijh}\right)^2 \lambda^*_{Qijh} + \left(n^s_{Dijh}\right)^2 \lambda^*_{Dijh}} \tag{11}$$

$$\lambda^*_{Qijh} = \frac{\left(\sigma^s_{Qijh}\right)^2}{\left(\sigma^s_{ijh}\right)^2};\quad \lambda^*_{Dijh} = \frac{\left(\sigma^s_{Dijh}\right)^2}{\left(\sigma^s_{ijh}\right)^2} \tag{13}$$

where σ^s_{Qijh} and σ^s_{Dijh} are the standard deviations of s'_{Qijh} and s'_{Dijh}, respectively; λ^*_{Qijh} and λ^*_{Dijh} are the normalized variances of the quasi-static and of the resonant part of the stress, respectively; they provide a measure of the relative importance of the two dominant spectral components of the stress power spectral density function. In Eqs. (11)-(13) the dependence on M is not made explicit for sake of simplicity.

The damage induced by all the wind loading conditions is evaluated collecting the wind loading cycles into a discrete cycles histogram [9]. Let us consider a series of stress amplitudes Δ_k (k=1,2,...); the discrete cycles histogram is defined as the mean number $\overline{n}_{ijhk}$ of stress cycles with amplitude Δ_k and mean stress $\overline{s}_{ijh}$; this quantity is a function of the mean wind velocity (i), of the wind direction (j) and of the Monin-Obukhov length (h). It is worth noting that $\overline{n}_{ijhk}$ is proportional to the effective time of the ijh-th loading condition, $T_{ijh} = TP_{ijh}$, and can be obtained by applying a suitable counting cycle method to the fluctuating stress process s'_{ijh}. Authors have recently proposed three cycle counting techniques for wind-induced actions. Two of them, namely the Peak Counting method and the Peak-Valley Counting method [8-9],

are based on the classic narrow-band assumption and furnishes an upper and a lower bound of damage, respectively. When the structural response is dominated by the fundamental mode of vibration, for example in resonant crosswind response, the two bounds are very close. On the contrary, when the quasi-static component of the response is relevant, for example in along-wind response, the gap between these two bounds may be very large, thus a more refined counting method was developed, based on the so called bi-modal assumption [9]; in this case, the low and the high-frequency spectral contents of the stress processes are associated, respectively, with the background and with the resonant part of the response.

The mean fraction of damage induced by the ijhk-th block of the cycles histogram can be evaluated adopting the Palmgren-Miner linear rule, given by:

$$\overline{d}_{ijhk}(T) = \frac{\overline{n}_{ijhk}(T)}{N_{ijhk}} \tag{1}$$

N_{ijhk} being the number of the stress cycles with amplitude Δ_k and mean stress $\overline{s}_{ijh}$ that causes the collapse. In accordance with Wohler's study, standards usually furnish the number of the stress cycles with amplitude Δ_k and zero mean stress that causes the collapse as a broken line in a log-log scale. Thus, the r-th segment of the modified Wohler's diagram is given by:

$$N_{ijhk} = \frac{a_r}{\left(\Delta_{e,ijhk}\right)^{b_r}} \qquad \text{for} \quad \Delta^{(r-1)} \le \Delta_{e,ijhk} \le \Delta^{(r)} \tag{4}$$

where a_r and b_r depend on the properties of the considered structural detail; $\Delta^{(r)}$ is the r-th term of a suitable series of discrete values of the stress amplitude cycles, $\Delta_{e,ijhk}$ is an equivalent amplitude, taking into account the non-zero mean stress.

Finally, the total mean damage is given by:

$$\overline{D}(T) = \sum_i \sum_j \sum_h \sum_k \overline{d}_{ijhk}(T) \tag{5}$$

Moreover, assuming that the collapse occurs when $\overline{D}$ reaches the unit, the mean fatigue life can be estimated by:

$$\hat{T}_F = \frac{1}{\overline{D}(1)} \tag{6}$$

where $\overline{D}(1)$ denotes the mean damage intensity, i.e. the mean damage per unit time.

3 CASE STUDY 1: ANEMOMETRIC POLE

The first examined structure is an anemometric pole, of total height h=10 m, composed by a steel shaft with octagonal section, which diameter varies linearly from 220 mm at bottom to 78 mm at top. The pole carries an anemometer at the top, a photovoltaic panel at z=9 m and a metallic box at z=2 m, represented as concentrated masses of 8 kg, 16 kg and 58 kg, respectively. This simple structure exhibited a premature collapse after one year from its installation, caused by a fatigue crack in the base welding joint (Fig. 1).

During its life, the anemometer registered continuously the ten-minutes mean wind velocity (Fig. 2 a). Adopting the procedure previously explained, the stress state and fatigue damage associated with the wind loading conditions is examined. The probability of occurrence of the loading conditions is associated only to the mean wind velocity variation, as no information about directional distribution and atmospheric stratification are measured at the site. Fig.

2 b shows the probability distribution of mean wind velocity obtained from the measured wind velocity time history. It can be noted that the maximum mean wind velocity measured at the top of the pole, $\overline{u}_{10}$= 32.5 m/s, is higher than the maximum wind velocity with 50 years of return period, evaluated at design stage, accordingly to the standard codes ($\overline{u}_{10}$= 28.2 m/s according to the national standard code [12]); it is also worth noting that the mean wind velocity $\overline{u}_{10}$= 28.2 m/s has been exceeded 3 times in one year in independent events. Thus, the site is characterized by windy conditions well above those prescribed by codes.

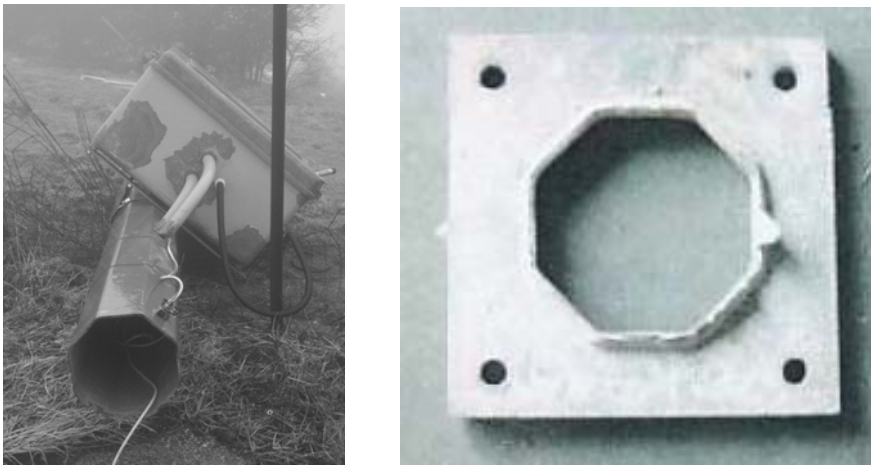

Figure 1: pictures of the collapsed pole.

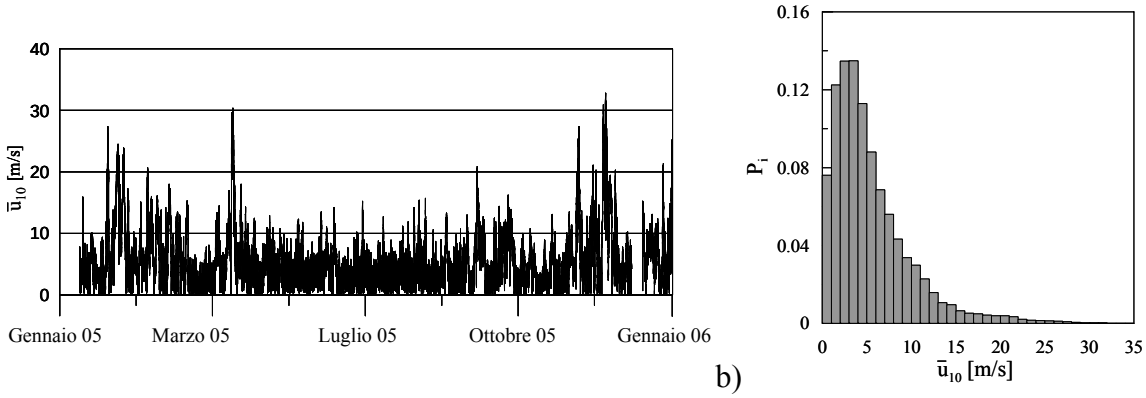

a) b)

Figure 2: a) measured wind velocity time history; b) wind velocity probability of occurrence.

The structure is schematized as a vertical cantilever beam. The fundamental frequency is n_1=0.54 Hz; the structural damping is assumed as ζ_1=0.005. The drag coefficient of the shaft is estimated as c_d=1.2. The alongwind and crosswind responses are evaluated taking into account turbulence and vortex shedding actions, on varying the mean wind velocity from 0 to 35 m/s with a velocity step of 1 m/s. Fig. 3 a shows the mean value $\overline{s}$ and the standard deviations σ_{sx} and σ_{sy} of the nominal stress at the base of the structure. As it can be noted, the alongwind and crosswind responses are mainly due to turbulence and grow with the mean wind velocity. The vortex shedding action has limited effects, as the critical wind velocity, $\overline{u}_{10,cr}$= 1.5 m/s, is very low. The alongwind action produces the stress value s_{max}=170 MPa, at the maximum registered wind velocity $\overline{u}_{10}$= 32.5 m/s, well below the yield limit of the material f_y=355 MPa (Table 1). Fig. 3 b shows the expected frequencies ν_{sx} and ν_{sy} of the nominal stress at the base of the structure. The expected frequency of the alongwind response grows with the mean wind velocity, however it is always well below the natural frequency of the

structure. This is due to the prevalence of the quasi-static part of the response. The expected frequency of the crosswind response reaches the natural frequency in correspondence of the critical wind velocity for vortex shedding excitation ($\bar{u}_{10,cr}$= 1.5 m/s). Outside the critical range, the crosswind expected frequency shows a trend similar to the alongwind one; however, the values are higher; this is due to the greater prevalence of the resonant part of the response, linked to the shift of the lateral turbulence spectral content towards higher frequency values.

The wind-induced fatigue damage has been evaluated adopting the procedure previously explained, expressing the cycle histograms by means of the bi-modal counting method [9-10]. The fatigue behavior of the critical section has been described by the S-N curves proposed by Eurocode 3 [13], assuming the detail category 36.

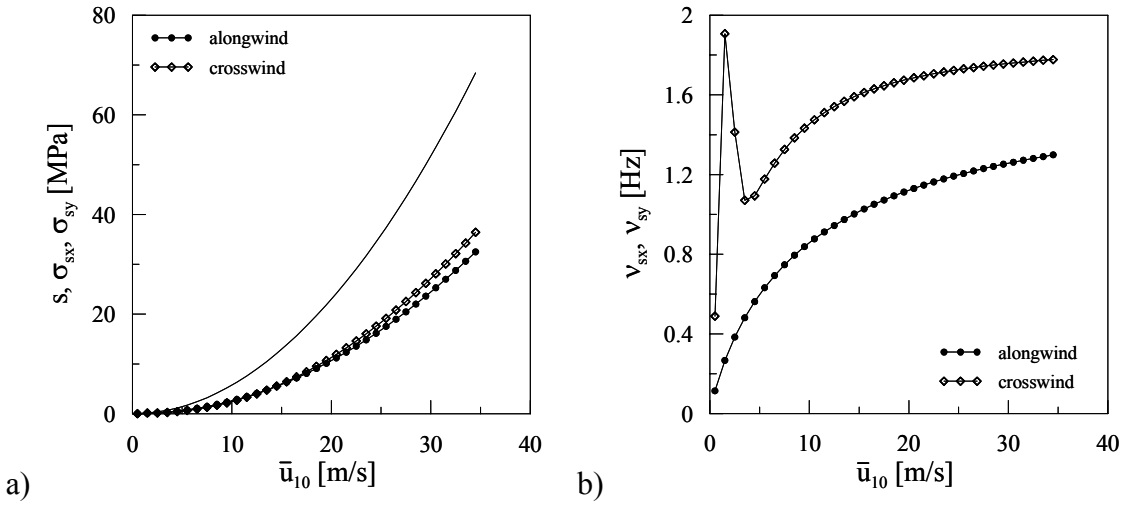

Figure 3: a) mean and standard deviation of stress; b) expected frequency of stress.

Fig. 4 shows the mean fractions of damage induced by the loading conditions on varying the wind velocity values. The alongwind and crosswind fatigue damage are concentrated in the range of high wind velocities, between 20 and 30 m/s.

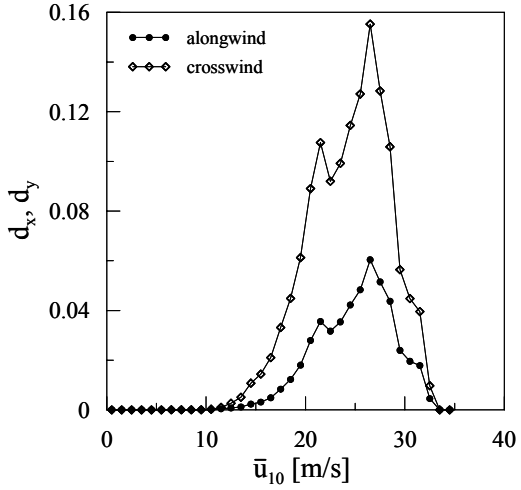

Figure 4: mean fractions of damage.

This result is quite anomalous with respect to other experiences with similar structures [10], in which the wind induced fatigue damage is usually concentrated in the range of moderate

wind velocities, between 10 and 20 m/s. This situation is a consequence of the windy condition of the site; in particular, it is due to a parent distribution of the wind velocity at the site shifted towards high wind velocities (Fig. 2 b).

It is worth noting that, while the alongwind action produces the maximum stress, the crosswind action produces the maximum fatigue damage; as the standard deviations of alongwind and crosswind fluctuating stresses are similar (Fig. 3 a), the difference in the induced fatigue damage is linked with the expected frequencies of the processes (Fig. 3 b).

Table 1 summarizes the maximum stress and the predicted fatigue life for alongwind, crosswind and simultaneous actions. The predicted fatigue life linked with alongwind, crosswind and simultaneous responses are obtained disregarding directional effects; however, the obtained values are very similar to the exhibited fatigue life.

	alongwind	crosswind	along+cross
s_{max} [MPa]	170	125	160
T_F [days]	740	270	374

Table 1: maximum stresses and predicted fatigue life.

It can be concluded that the collapse is linked with a particular windy condition of the site. The safety factor adopted in structural design covers this anomalous situation from the ultimate limit state point of view, while it is completely inadequate from the fatigue point of view.

4 CASE STUDY 2: ANTENNAS TOWER

The second examined structure is an antennas tower, of total height h=30 m. It is composed by a steel shaft with polygonal section, 24 m high, which diameter varies linearly from 1100 mm at bottom to 550 mm at top. Above the steel shaft there is a steel bar with circular section, 6 m high, which diameter is constant and equal to 119 mm. The bar at the top can support different configurations of telecommunication antennas. The antennas can be covered by a fiberglass cylinder with diameter of 1500 mm, for aesthetic reasons.

The configuration with the cover cylinder exhibited a premature collapse, caused by a fatigue crack at the shaft-bar joint. Moreover, a lot of similar antennas towers were interested by large fatigue damage, showing a critical behavior of the same structural type. Adopting the procedure previously explained, the evolution of the stress state and fatigue damage of the tower with the cover cylinder (C1) (Fig. 6 a) and without the cover cylinder (C2) (Fig. 6 c) is examined. As no direct measurement of the wind velocity is available at the site, adopting the national standard code [12] the reference wind velocity with 50 years of return period is assumed as $\overline{u}_{ref}$ = 27 m/s, the roughness length is z_0=0.05 m and the topography coefficient is c_T=1. The probability of occurrence of the loading conditions (Fig. 5), associated only with the mean wind velocity variation, is based on a Weibull distribution characterized by probability of zero values of wind velocity F_0=0.4, and parameters k = 1.32 and c = 3.75 m/s.

The structure is schematized as a cantilever beam, taking into account the different stiffness of the shaft and of the upper bar, and the different mass distribution of the considered configurations. The natural frequencies are reported in Table 2. It can be noted that the configuration without the cover cylinder (C2) is characterised by higher natural frequencies, as the structural mass is reduced.

Fig. 6 shows the natural modes of vibrations of the configurations C1 (Fig. 6 a and b) and C2 (Fig. 6 c and d). The natural modes vary slowly in the two configurations. In both cases the second mode presents a particular trend, with a maximum at the top of the polygonal part of the shaft and a typical first mode-shape in correspondence of the supporting bar.

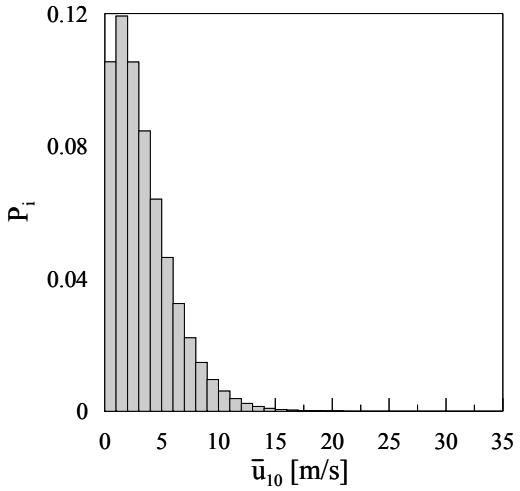

Figure 5: wind velocity probability of occurrence.

Configuration	n_1 (Hz)	n_2 (Hz)	n_3 (Hz)
C1	0.92	2.84	7.46
C2	1.09	3.90	7.69

Table 2: natural frequencies of the tower.

The structural damping is assumed as $\zeta_k = 0.004$ for each mode of vibration. The drag coefficient of the structure is evaluated taking into account the contribution of the different parts of the two configurations and its dependence on the Reynolds number. The drag coefficient of the polygonal part of the shaft has been estimated as c_d=1.15 for $\bar{u}_{10} \leq 3.5$ m/s and c_d=0.74 for $\bar{u}_{10} > 3.5$ m/s. The drag coefficient of the cover cylinder (C1) is c_d=0.5 for the considered range of wind velocity. The drag coefficient of the antennas mounted on the supporting bar without the cover cylinder (C2) strictly depends on the shape and the number of the mounted antennas. Based on a series of wind tunnel tests, the estimated drag coefficient of the considered configuration is c_d=0.6 (referred to the diameter of the cover cylinder). Moreover, the angular derivative of the lift coefficient is c_l'=0.45.

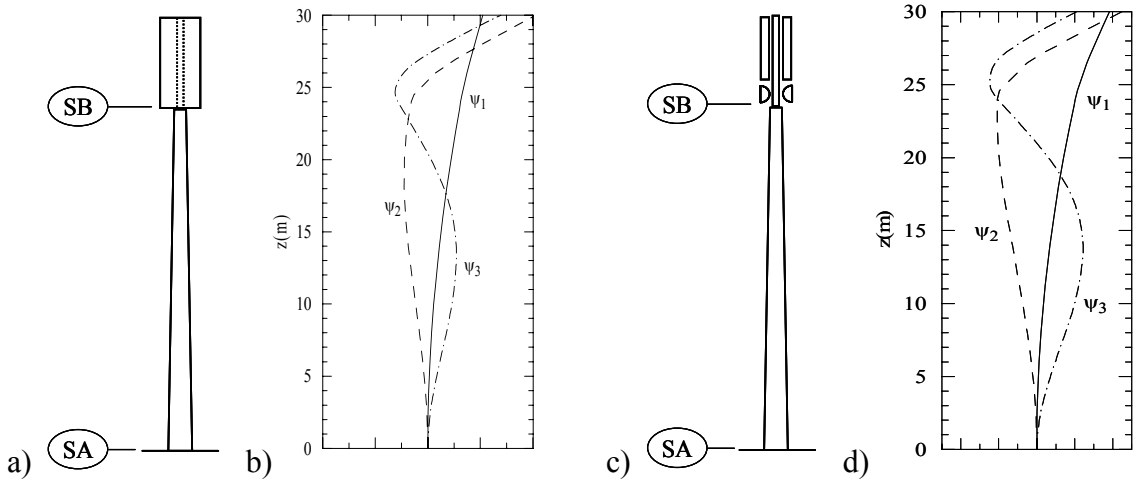

Figure 6: a) scheme of the antennas tower with the cylinder (C1); b) Natural modes of vibration the antennas tower with the cylinder (C1); c) scheme of the antennas tower without the cylinder (C2); d) Natural modes of vibration the antennas tower without the cylinder (C2).

The vortex shedding actions can produce relevant forcing mechanisms under different resonance conditions. For C1 configuration, two critical situations can arise: the first corresponds to the vortex shedding resonant with the tower vibration modes in correspondence of the cover cylinder (1); the second corresponds to the vortex shedding resonant with the tower vibration modes in correspondence of the top of the polygonal part of the shaft (2). Table 3 reports the critical velocity and the Scruton number associated with the first three modes of vibration, for the two considered conditions. In particular, Scruton numbers show that the hypothesis (1) is related with potentially very critical states for the tower.

mode k	v_k (m/s) (1)	Sc_k (1)	v_k (m/s) (2)	Sc_k (2)
1	6.90	2.52	3.04	13.01
2	21.30	2.59	9.37	13.29
3	-	-	24.62	11.88

Table 3: critical wind velocity and Scruton number related with resonant vortex shedding from the cover cylinder (1) and from the polygonal part of the shaft (2) for C1 configuration.

In the C2 configuration, the only critical situation is related to the vortex shedding resonant with the tower vibration modes in correspondence of the top of the polygonal part of the shaft. Table 4 reports the critical velocity and the Scruton number associated with the first three modes of vibration.

Mode k	v_k (m/s)	Sc_k
1	3.58	11.91
2	11.70	10.71
3	23.07	13.02

Table 4: critical wind velocity and Scruton number related with resonant vortex shedding from the polygonal part of the shaft for C2 configuration.

The analysis of the structural response puts in evidence two potentially critical sections, at the base of the tower (SA) and at the base of the supporting bar (SB), respectively (see Fig. 6).

For the C1 configuration, the crosswind response is largely prevalent with respect to alongwind response. The Fig. 7 a shows the standard deviation σ_{sy} of the nominal stress states for the C1 configuration, on varying the mean wind velocity. The C1 response in both the considered sections is dominated by the crosswind actions, resonant with the first mode at u_{cr}= 6 m/s and with the second mode at u_{cr}= 18 m/s. Thus, it is evident that the main forcing action is due to the vortex shedding resonant with the tower vibration modes in correspondence of the cover cylider (1). Moreover, it can be noted that the most critical section is at the base of the supporting bar (SB). In this section, the C1 maximum stress value associated wirth the first critical velocity is s_{max}=220 MPa, below the yield limit of the material f_y=355 MPa (Table 5); the C1 maximum stress associated to the second critical velocity is near to the yield limit of the material; the analysis of this condition is affected by large uncertainties and, in principle, would require deeper evaluations; this is not necessary for the consideration reported below.

The wind-induced fatigue damage in the critical sections has been evaluated adopting the procedure previously explained. The fatigue behavior of the critical sections has been de-

scribed by the S-N curves proposed by Eurocode 3 [13], assuming the detail category 50. Fig. 7 b shows the mean fractions of the damage induced by the loading conditions on varying the wind velocity values, in the critical section SB at the base of the supporting bar. The crosswind fatigue damage is concentrated in the range of the first critical velocity, u_{cr}= 6 m/s, showing that in this case the fatigue damage is mainly linked with the vortex shedding resonant with the first mode, as the associated loading conditions are characterized by high stress states and high probability of occurrence. The vortex shedding resonant with the second mode may produce high stress states (Fig. 7 a), however, the associated loading conditions are characterized by low probability of occurrence, thus inducing low fatigue damage on the structure.

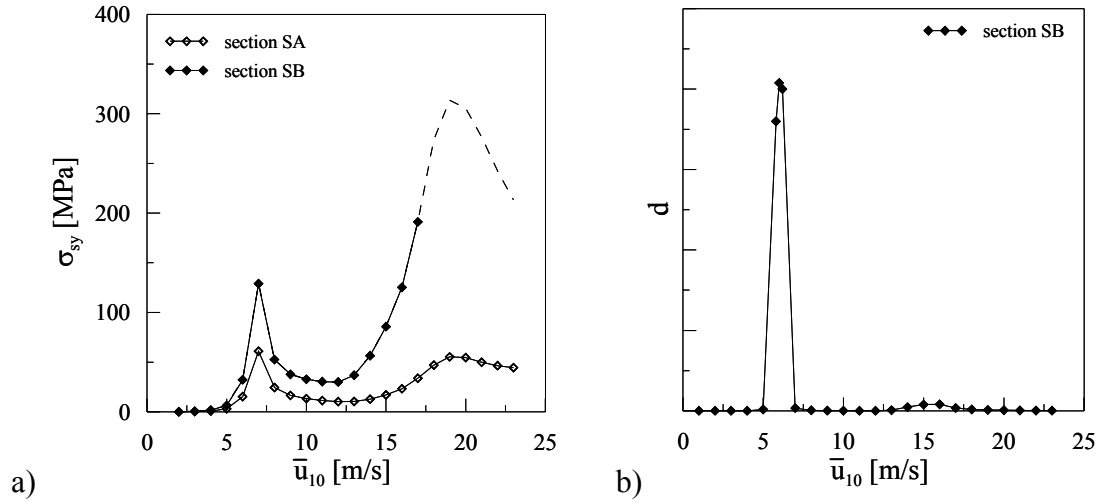

Figure 7: a) standard deviation of C1 crosswind stress; b) C1 mean fractions of damage in section SB.

Fig. 8 a shows the mean value $\bar{s}$ and the standard deviations σ_{sx} and σ_{sy} of the nominal stress for the C2 configuration in the critical section SB. As it can be noted, the C2 response in alongwind and crosswind directions grows with the mean wind velocity; vortex shedding effects are drastically reduced and the crosswind response is qualitatively changed by the cover cylinder remove. The C2 alongwind action produces the maximum stress value s_{max}=137 MPa, at the reference wind velocity $\bar{u}_{10}$= 27 m/s, below the yield limit of the material f_y=355 MPa (Table 5).

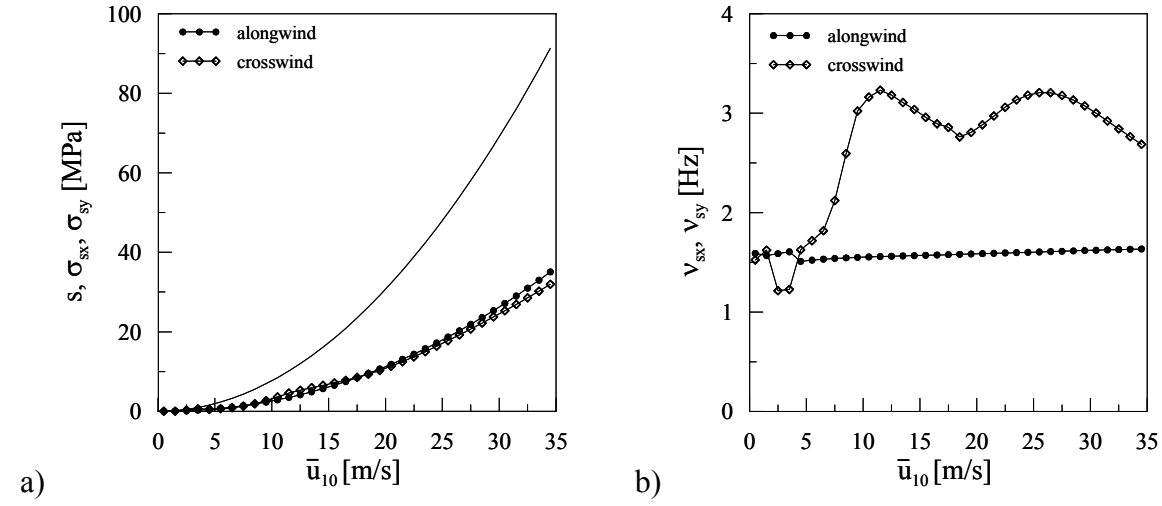

Figure 8: a) C2 mean and standard deviations and b) C2 expected frequency of stress in section SB.

Fig. 8 b shows the expected frequencies ν_{sx} and ν_{sy} of the nominal stress in the critical section SB. The expected frequency of the alongwind response grows with the mean wind velocity, however it is always below the natural frequency of the structure. This is due to the prevalence of the quasi-static part of the response. The expected frequency of the crosswind response puts in evidence the contribution of vortex shedding actions resonant to the first and second modes.

The wind-induced fatigue damage in the critical section SB has been evaluated adopting the procedure previously explained. The fatigue behavior of the critical section has been described by the S-N curves proposed by Eurocode 3 [13], assuming the detail category 50.

Fig. 9 shows the mean fractions of damage induced by the loading conditions on varying the wind velocity values. The C2 alongwind and crosswind fatigue damage are concentrated in the range of moderate and frequent wind velocities, between 10 and 20 m/s. The C2 fatigue damage is mainly linked with the crosswind actions. As the standard deviations of alongwind and crosswind fluctuating stresses are similar (Fig. 8 a), the difference is linked with the expected frequencies of the processes (Fig. 8 b).

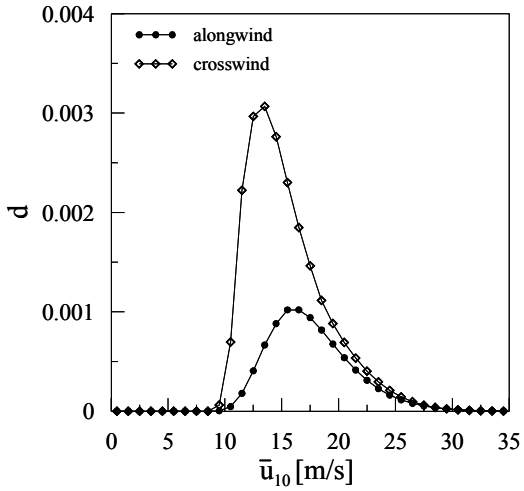

Figure 9: C2 mean fractions of damage in section SB.

Table 5 summarizes the maximum stress and the predicted fatigue life for the two considered configurations. In C1 configuration, the resulting fatigue life is very low (Table 5), coherently with the exhibited fatigue life of the real structure. In C2 configuration, the minimum predicted fatigue life is near 50 years (Table 5), considerably higher than in C1 case.

	C1 crosswind	C2 alongwind	C2 crosswind
s_{max} [MPa]	220 (1 mode)	137	80.5
T_F	< 1 year	115 years	45 years

Table 5: maximum stresses and predicted fatigue life.

It can be concluded that fatigue damage observed in C1 towers are linked with the aerodynamic effects generated by the cover cylinder. Removing the cover cylinder (C2), the aerodynamic actions are completely changed and the vortex shedding effects are drastically reduced. The analysis highlight two critical sections, at the base of the tower (SA) and at the base of the supporting bar (SB). However, the maximum fatigue damage is in the section (SB) for both configurations, showing that the joint of the shaft with the bar, two elements characterized by very different stiffness, can result as critical.

5 CONCLUSIONS

The authors of this paper have recently proposed a complete procedure for wind-induced fatigue analysis of slender structures, which requires the evaluation of the wind loading effects and damage associated with all loading conditions. The proposed method has been applied to analyze the wind-induced collapses of two real slender structures, a ten meters anemometric pole and a thirty meters antennas tower. Both the structures are characterized by a very simple structural scheme and they both satisfy the national and international Structural Codes from the ultimate limit state point of view. The application of the proposed method furnishes a predicted fatigue life very similar to the exhibited behavior of both structures. Moreover, it gives a picture of the evaluation of the stress state and wind-induced damage of the structure, furnishing useful information on the structural behavior and a key for the interpretation of collapse and damage causes.

The anemometric pole collapse is linked with a particular windy condition of the site. The safety factor adopted in structural design covers this anomalous situation from the ultimate limit state point of view, while it is completely inadequate from the fatigue point of view.

The antennas tower damage and collapse are linked with aerodynamic effects generated by the vortex shedding actions resonant with the top cover cylinder. Removing the cover cylinder, the vortex shedding effects are drastically reduced and the maximum stress value is linked with alongwind actions. However, even in this case, the crosswind actions due to turbulence and vortex shedding actions are responsible of the main fatigue damage; as the standard deviations of alongwind and crosswind fluctuating stresses are similar, this result is linked with the larger expected frequencies of the crosswind processes.

From a general point of view, the analysis puts in evidence the good agreement between the predicted and exhibited values of the fatigue life of the considered structures, confirming the reliability of the proposed method. Even more, it highlights the limits of Standards and Codes in preventing wind-induced damage. Thus it suggests, as a perspective of this work, the introduction of a simplified procedure to apply in engineering and standards provision, based on an advanced closed form solution of wind-induced fatigue damage.

REFERENCES

[1] A.P. Robertson, R.P. Hoxey, J.L. Short, L.R. Burges, B.W. Smith and R.H.Y. Ko, Wind-induced fatigue loading of tubular steel lighting columns, *Wind and Structures*, **4**,163-176, 2001.

[2] U. Peil and M. Behrens, Fatigue of tubular steel lighting columns under wind load, *Wind and Structures*, **5**, 463-478, 2002.

[3] L. Caracoglia and N.P. Jones, Wind-induced failures of highway light poles during winter storms, Proceedings of the ASME Pressure Vessels and Piping Division Conference, Vancouver, BC, Canada, July 23-27, 2006.

[4] B. N. Pritchard, Steel chimney oscillations: a comparative study of their reported performance versus predictions using existing design techniques, *Engineering Structures*, **6**, 315-323, 1984.

[5] C. Verwiebe and A. Glockner, Failure of steel chimneys due to vortex excited vibrations in the second mode, Proceedings of the XI ICWE, Texas Tech University, Lubbock, 2003.

[6] M.P. Repetto and G. Solari, Dynamic alongwind fatigue of slender structures, *Engineering Structures*, **22**, 1622-1633, 2001.

[7] M.P. Repetto and G. Solari, Dynamic crosswind fatigue of slender structures, *Wind and Structures*, **5**, 527-542, 2002.

[8] M.P. Repetto and G. Solari, Directional wind-induced fatigue of slender vertical structures, *Journal of Structural Engineering, ASCE*, **130**, 1032-1040, 2004.

[9] M.P. Repetto, Cycles counting methods for bi-modal stationary Gaussian processes, *Probabilistic Engineering Mechanics*, **20**, 229-238, 2005.

[10] M.P. Repetto, G. Solari. Bimodal alongwind fatigue of structures. *Journal of Structural engineering*, *ASCE***, 132**, 899–908, 2006.

[11] M.P. Repetto, G. Solari. Wind-induced fatigue of structures under neutral and non-neutral atmospheric conditions. *Journal of Wind Engineering and Industrial Aerodynamics*, **95**, 1364–1383, 2007.

[12] Decreto 16 gennaio 1996 del Ministero dei Lavori Pubblici, Norme tecniche relative ai "Criteri generali per la verifica di sicurezza delle costruzioni e dei carichi e sovraccarichi", Italy, 1996.

[13] Eurocode 3, *Design of steel structures*, European Standard, prENV 1993, 1994.